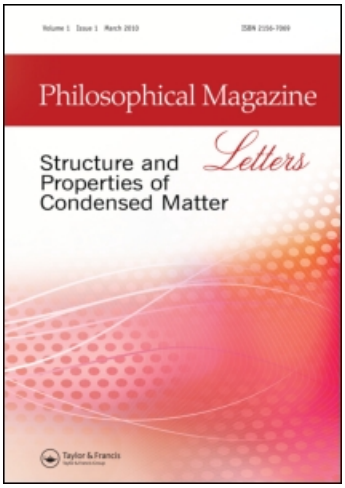

Philosophical Magazine Letters
Publication details, including instructions for authors and subscription information:
http://www.informaworld.com/smpp/title~content=t713695410

Wave propagating across atomic-continuum interface

Xianqiao Wang[a]; James D. Lee[a]
[a] Department of Mechanical and Aerospace Engineering, George Washington University, Washington, DC 20052, USA

First published on: 07 March 2011

To cite this Article Wang, Xianqiao and Lee, James D.(2011) 'Wave propagating across atomic-continuum interface', Philosophical Magazine Letters, 91: 5, 375 — 386, First published on: 07 March 2011 (iFirst)
To link to this Article: DOI: 10.1080/09500839.2011.562473
URL: http://dx.doi.org/10.1080/09500839.2011.562473

Philosophical Magazine Letters
Vol. 91, No. 5, May 2011, 375–386

Taylor & Francis
Taylor & Francis Group

Wave propagating across atomic–continuum interface

Xianqiao Wang and James D. Lee*

Department of Mechanical and Aerospace Engineering, George Washington University, Washington, DC 20052, USA

(*Received 9 April 2010; final version received 9 February 2011*)

Motivated by eliminating the spurious wave reflection at the interface between atomic and continuum domains in the multiscale modeling and simulation, we present a novel numerical approach for the atomistic field theory without any special treatment at the interfaces. This novel approach abandons the method to calculate the finite element nodal forces in the continuum domain based on the strain–stress relation. Instead, it employs the interatomic forces as in molecular dynamics simulation. This nonlocal procedure overcomes the force mismatch between atomic and continuum domains and enables a seamless scale transition between fully atomistic resolution and continuum description. Meanwhile, to balance the trade-off between computational efficiency and numerical accuracy, we adopt a cluster-based sampling scheme which allows a group of unit cells around every nodal point to contribute to the calculation of nodal forces. Numerical results show that this novel numerical procedure drastically reduces the wave reflection at the atomic–continuum interface.

Keywords: wave propagation; multiscale material modeling; atomic–continuum interface; nanomechanics; atomistic field theory

1. Introduction

In recent years, a great deal of interests has been focused on developing concurrent multiscale modeling methods that are capable of reproducing the results of a full atomistic simulation at a reduced computational cost. Despite widespread interests and efforts, major challenges exist for the simulation of nano/micro-scale systems over a realistic range of time, length, temperature as well as in multiple physical conditions and environments. The most formidable challenge that arises in such concurrent multiscale modeling is interfacing molecular dynamics (MD) with continuum mechanics [1–4]. In the traditional coupled atomistic–continuum models, only the acoustic phonons can be reproduced in the continuum region such that they have much smaller cutoff frequencies than the MD model. As a result, a difficulty arises in such concurrent multiscale couplings when the high-frequency parts of waves are often spuriously reflected at the molecular/continuum interface. These spurious reflections can be explained by noting that for a wave greater than the cutoff frequency of the continuum model, the interface appears as an almost

*Corresponding author. Email: jdlee@gwu.edu

ISSN 0950–0839 print/ISSN 1362–3036 online

DOI: 10.1080/09500839.2011.562473
http://www.informaworld.com

rigid boundary. So instead of smoothly propagating into the continuum model, the high-frequency part of the wave is reflected. This results in spurious growth of energy in the molecular domain [5]. In order to minimize the wave reflections at the atomic–continuum interface, a number of coupling schemes or boundary conditions have been proposed, such as the viscous damping treatment and the physically motivated description of coupling across the interface [6–10]. In this letter, we present a new numerical approach for atomistic field theory (AFT), which offers the possibility to eliminate the spurious wave reflection at the interface between atomic and continuum regions.

2. Atomistic field theory

To provide the background for the subsequent developments, we briefly review the AFT developed by Chen and Lee [11] and its corresponding numerical algorithm by Lee et al. [12]. Note that a crystalline material is distinguished from other states of matter by a periodic arrangement of the atoms, depicted in Figure 1. Following the concepts of classical statistical mechanical approach [13], a crystalline material can be viewed as a continuous collection of lattice cells and a group of discrete atoms situated within each lattice cell. A more general link, shown in Figure 2, between any phase space function $\mathbf{A}(\mathbf{r}, \mathbf{p})$ and the corresponding local density function $\mathbf{a}(\mathbf{x}, \mathbf{y}^{\alpha}, t)$ was developed by Chen [5] as

$$\mathbf{a}(\mathbf{x}, \mathbf{y}^{\alpha}, t) = \sum_{k=1}^{N_l} \sum_{\xi=1}^{N_a} \mathbf{A}(\mathbf{r}, \mathbf{p}) \delta(\mathbf{R}^k - \mathbf{x}) \tilde{\delta}(\Delta \mathbf{r}^{k\xi} - \mathbf{y}^{\alpha}) \quad (\alpha = 1, 2, 3, \ldots, N_a), \tag{1}$$

where $\mathbf{r}$ and $\mathbf{p}$ are the positions and momenta of atoms in the phase space, respectively; the superscript $k\xi$ refers to the ξth atom in the kth unit cell; $\mathbf{R}^k$ is the position of the mass center of the kth unit cell; $\Delta \mathbf{r}^{k\xi}$ is the atomic position of the ξth

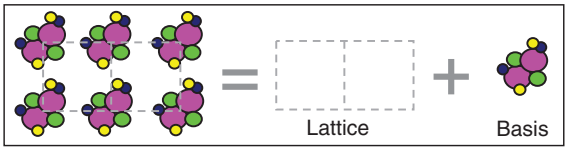

Figure 1. Atomistic view of crystal structure.

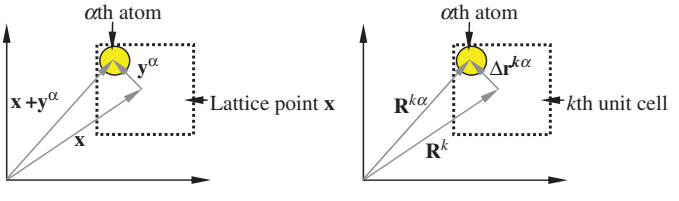

Figure 2. Relation between physical space and phase space descriptions.

atom relative to the mass center of the kth unit cell; $\mathbf{x}$ and $\mathbf{y}^\alpha$ are the corresponding physical space counterparts of $\mathbf{R}^k$ and $\Delta\mathbf{r}^{k\alpha}$; N_l is the total number of unit cells in the system; N_a is the number of atoms in a unit cell; t is the time of physical space. The first delta function in Equation (1) is a localization function. It can be a Dirac δ-function [14], or a distribution function [15]. The field descriptions of the conservation equations and the constitutive relations have been proved to be independent of the choices of the localization function [16]. The second delta function in Equation (1) is the Kronecker delta, which identifies $\mathbf{y}^\alpha$ to $\Delta\mathbf{r}^{k\alpha}$.

By means of Equation (1), the local density quantities, such as mass density ρ^α, linear momentum density $\rho^\alpha(\mathbf{v}+\Delta\mathbf{v}^\alpha)$, interatomic force density $\mathbf{f}^\alpha$ and external force density $\boldsymbol{\varphi}^\alpha$ are defined in [11,12]. In the case of ''one-way coupling'', the temperature is given as a function of space and time. The relevant governing equations are just the balance law for linear momentum, i.e.,

$$\rho^\alpha\ddot{\mathbf{u}}^\alpha(\mathbf{x},t)=\mathbf{f}_t^\alpha(\mathbf{x},t)+\mathbf{f}^\alpha(\mathbf{x},t)+\boldsymbol{\varphi}^\alpha(\mathbf{x},t), \tag{2}$$

where $\dot{\mathbf{u}}^\alpha(\mathbf{x},t)=\mathbf{v}+\Delta\mathbf{v}^\alpha$; $\mathbf{f}_t^\alpha(\mathbf{x},t)$ is the force density acting on the αth atom due to temperature. The existence of superscript α in Equation (2) implies that the atomic information is naturally built in AFT, thereby eliminating the mismatch of phonon descriptions in atomic and continuum regions. Therefore AFT is inherently suitable for complex crystals, which is quite different from the classical continuum field theory.

In lattice systems, the smallest allowable physical volume in AFT is the volume of a unit cell. The mass density of the αth atom at $\mathbf{x}$ is thus $\rho^\alpha(\mathbf{x},t)=m^\alpha/\Delta V(\mathbf{x},t)$, where m^α is the mass of the αth atom and ΔV is the volume of unit cell. Consider the body as a material system made of two regions: continuum region (N_l unit cells) and atomic region (N atoms), as shown in Figure 3 (here a 2-D picture is shown for the purpose of illustration; the atomic region is shown with color points, different color refers to different kinds of atoms; notice that the continuum region and the atomic regions are not drawn to scale). Each unit cell (a square in Figure 3) has N_a atoms in

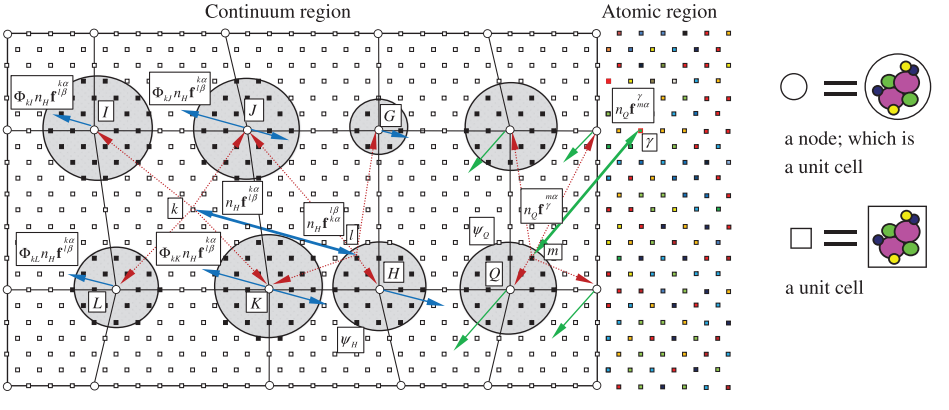

Figure 3. Schematic picture of AFT model with force distributions.

the continuum region. Then the governing equation in these two regions can be expressed as

Continuum region $[\alpha = 1, 2, 3, \ldots, N_a]$

$$m^{\alpha}\ddot{\mathbf{u}}^{\alpha}(\mathbf{x}, t) = \mathbf{F}^{\alpha}_{tC}(\mathbf{x}, t) + \mathbf{F}^{\alpha}_{C}(\mathbf{x}, t) + \mathbf{\Phi}^{\alpha}_{C}(\mathbf{x}, t), \tag{3}$$

where $\mathbf{F}^{\alpha}_{C}(\mathbf{x}, t)$ is the interatomic force; $\mathbf{F}^{\alpha}_{tC}(\mathbf{x}, t)$ is the interatomic force due to temperature and $\mathbf{\Phi}^{\alpha}_{C}(\mathbf{x}, t)$ is the force due to external fields.

Atomic region $[\beta = 1, 2, 3, \ldots, N]$

$$m^{\beta}\ddot{\mathbf{u}}^{\beta}(\mathbf{x}, t) = \mathbf{F}^{\beta}_{A}(t) + \mathbf{\Phi}^{\beta}_{A}(\mathbf{x}, t), \tag{4}$$

where $\mathbf{F}^{\beta}_{A}(t)$ and $\mathbf{\Phi}^{\beta}_{A}(t)$ are the interatomic force and external force acting on the βth atom, respectively. It is seen that, in MD simulation, temperature is not an independent variable; hence it does not appear in the governing equations; instead it is calculated as

$$3Nk_B T = \sum_{i=1}^{n} m^i(\dot{\mathbf{u}}^i - \bar{\dot{\mathbf{u}}}) \cdot (\dot{\mathbf{u}}^i - \bar{\dot{\mathbf{u}}}), \tag{5}$$

where $\bar{\dot{\mathbf{u}}}$ is the mass-weighted velocity of a group of n atoms, k_B is the Boltzmann constant and T is the temperature of a group of atoms.

Define $\mathbf{f}^{\xi\eta}[\mathbf{u}^{\xi}, \mathbf{u}^{\eta}]$ as the interatomic force acting on an atom whose type and position are indicated by ξ and $\mathbf{u}^{\xi}$:

$$\mathbf{f}^{\xi\eta}[\mathbf{u}^{\xi}, \mathbf{u}^{\eta}] = -\frac{1}{2}\left(\frac{\partial U^{\xi\eta}}{\partial \mathbf{u}^{\xi}} - \frac{\partial U^{\xi\eta}}{\partial \mathbf{u}^{\eta}}\right) = \frac{1}{2}(\mathbf{f}^{\xi\eta} - \mathbf{f}^{\eta\xi}), \tag{6}$$

where $U^{\xi\eta}$ is the interatomic potential between the ξth atom and ηth atom.

For material systems that involve pair atomic interactions, the interatomic force $\mathbf{F}^{\alpha}_{C}(\mathbf{x}, t)$ in continuum region and $\mathbf{F}^{\beta}_{A}(t)$ in atomic region can be expressed, respectively, as

$$\mathbf{F}^{\alpha}_{C}(\mathbf{x}, t) = \int_{\Omega(\mathbf{x}', t)} \frac{1}{\Delta V(\mathbf{x}', t)} \sum_{\beta=1}^{N_a} \mathbf{F}^{\alpha\beta}\big[\mathbf{u}^{\alpha}(\mathbf{x}, t), \mathbf{u}^{\beta}(\mathbf{x}', t)\big] \mathrm{d}\Omega(\mathbf{x}', t) + \sum_{\beta=1}^{N} \mathbf{F}^{\alpha\beta}\big[\mathbf{u}^{\alpha}(\mathbf{x}, t), \mathbf{u}^{\beta}(t)\big], \tag{7}$$

$$\mathbf{F}^{\beta}_{A}(t) = \int_{\Omega(\mathbf{x}, t)} \frac{1}{\Delta V(\mathbf{x}, t)} \sum_{\alpha=1}^{N_a} \mathbf{F}^{\beta\alpha}\big[\mathbf{u}^{\beta}(t), \mathbf{u}^{\alpha}(\mathbf{x}, t)\big] \mathrm{d}\Omega(\mathbf{x}, t) + \sum_{\alpha=1}^{N} \mathbf{F}^{\beta\alpha}[\mathbf{u}^{\beta}(t), \mathbf{u}^{\alpha}(t)]. \tag{8}$$

It is noticed that, in Equations (7) and (8), full-blown nonlocality and atom-based constitutive relation are automatically rooted in the force calculation. So we have proposed a fully nonlocal AFT formulation.

3. Numerical methodology

In order to solve the above-mentioned material system efficiently and accurately, following the works of Miller et al. [14], Tadmor et al. [15] and Knap and Ortiz [16],

we introduce two approximations. The first one is a kinematic constraint aiming at the reduction of degrees of freedom by virtue of the shape function in the finite element (FE) method. The second one regards to the calculation of nodal forces in clusters with a specified summation rules. This cluster summation rules are taken as a compromise between numerical accuracy and computational efficiency.

The important part of this novel numerical approach is to reduce the degrees of freedom by the kinematic constraint. Some judiciously selected unit cells, called representative unit cells or rep-cells, retain their independent degrees of freedom. Each node in FE mesh is a rep-cell. The nodal displacements together with shape functions are employed to determine a displacement field, in other words, all other unit cells are forced to follow the motion of the nodes – this is what we called ''kinematic constraint'', which is the practice used in every FE analysis. The continuous displacement field $\mathbf{u}^{\alpha}(\mathbf{x})$ is approximated by FE interpolation from its nodal values $\mathbf{U}_I^{\alpha}$ as

$$\mathbf{u}^{\alpha}(\mathbf{x}) = \sum_{I=1}^{N_d} \Phi_I(\mathbf{x})\mathbf{U}_I^{\alpha}, \tag{9}$$

where $\Phi_I(\mathbf{x})$ is the shape function and N_d is the number of nodes in each element. After lengthy but straightforward derivations, finally we have [12]

Continuum region

$$\begin{aligned}\int_{\Omega(\mathbf{x})} \frac{1}{\Delta V(\mathbf{x})} m^{\alpha} \mathbf{\Phi}_J \mathbf{\Phi}_I \ddot{\mathbf{U}}_I^{\alpha} \mathrm{d}\Omega(\mathbf{x}) - \int_{\Omega(\mathbf{x})} \frac{1}{\Delta V(\mathbf{x})} \mathbf{\Phi}_J \\ \times \sum_{\beta=1}^{N_a} \int_{\Omega(\mathbf{x}')} \frac{1}{\Delta V(\mathbf{x}')} \mathbf{F}^{\alpha\beta}\Big[\mathbf{\Phi}_I \mathbf{U}_I^{\alpha}, \mathbf{\Phi}_K(\mathbf{x}')\mathbf{U}_K^{\beta}\Big] \mathrm{d}\Omega(\mathbf{x}')\mathrm{d}\Omega(\mathbf{x}) \\ - \int_{\Omega(\mathbf{x})} \frac{1}{\Delta V(\mathbf{x})} \mathbf{\Phi}_J \sum_{\beta=1}^{N} \mathbf{F}^{\alpha\beta}[\mathbf{\Phi}_I \mathbf{U}_I^{\alpha}, \mathbf{u}^{\beta}] \mathrm{d}\Omega(\mathbf{x}) - \int_{\Omega(\mathbf{x})} \frac{1}{\Delta V(\mathbf{x})} (\mathbf{F}_{tC}^{\alpha} + \mathbf{\Phi}_C^{\alpha}) \mathbf{\Phi}_J \mathrm{d}\Omega(\mathbf{x}) = 0,\end{aligned} \tag{10}$$

i.e.

$$\tilde{\mathbf{M}}_{IJ} \ddot{\mathbf{U}}_I^{\alpha} = \tilde{\mathbf{F}}_J^{\alpha} + \tilde{\mathbf{F}}_{tJ}^{\alpha} + \tilde{\mathbf{\Phi}}_J^{\alpha}, \tag{11}$$

where

$$\tilde{\mathbf{M}}_{IJ} = \int_{\Omega(\mathbf{x})} \frac{1}{\Delta V(\mathbf{x})} m^{\alpha} \Phi_J \Phi_I \mathrm{d}\Omega(\mathbf{x}), \tag{12}$$

$$\begin{aligned}\tilde{\mathbf{F}}_J^{\alpha} = \int_{\Omega(\mathbf{x})} \frac{1}{\Delta V(\mathbf{x})} \Phi_J \sum_{\beta=1}^{N_a} \int_{\Omega(\mathbf{x}')} \frac{1}{\Delta V(\mathbf{x}')} \mathbf{F}^{\alpha\beta}\Big[\Phi_I \mathbf{U}_I^{\alpha}, \Phi_K(\mathbf{x}')\mathbf{U}_K^{\beta}\Big] \mathrm{d}\Omega(\mathbf{x}')\mathrm{d}\Omega(\mathbf{x}) \\ + \int_{\Omega} \frac{1}{\Delta V(\mathbf{x})} \Phi_J \sum_{\beta=1}^{N} \mathbf{F}^{\alpha\beta}\big[\Phi_I \mathbf{U}_I^{\alpha}, \mathbf{u}^{\beta}\big] \mathrm{d}\Omega(\mathbf{x}),\end{aligned} \tag{13}$$

$$\tilde{\mathbf{F}}_{tJ}^{\alpha} = \int_{\Omega(\mathbf{x})} \frac{1}{\Delta V(\mathbf{x})} \mathbf{F}_{t}^{\alpha} \Phi_J \mathrm{d}\Omega(\mathbf{x}), \tag{14}$$

$$\tilde{\mathbf{\Phi}}_{J}^{\alpha} = \int_{\Omega(\mathbf{x})} \frac{1}{\Delta V(\mathbf{x})} \mathbf{\Phi}_{C}^{\alpha} \Phi_J \mathrm{d}\Omega(\mathbf{x}), \tag{15}$$

where $\tilde{M}_{IJ}$ is the mass matrix of the system; $\tilde{\mathbf{F}}_{J}^{\alpha}$, $\tilde{\mathbf{F}}_{tJ}^{\alpha}$, and $\tilde{\mathbf{\Phi}}_{J}^{\alpha}$ are the interatomic force, temperature force, and external force acting on the αth atom in the Jth node, respectively.

Atomic region

$$m^{\beta}\ddot{\mathbf{u}}^{\beta} - \mathbf{\Phi}_{A}^{\beta} - \sum_{\alpha=1}^{N} \mathbf{F}^{\beta\alpha}[\mathbf{u}^{\beta}, \mathbf{u}^{\alpha}] - \int_{\Omega(\mathbf{x})} \frac{1}{\Delta V(\mathbf{x})} \sum_{\alpha=1}^{N_a} \mathbf{F}^{\beta\alpha}[\mathbf{u}^{\beta}, \Phi_I \mathbf{U}_I^{\alpha}] \mathrm{d}\Omega(\mathbf{x}) = 0. \tag{16}$$

All integrals in Equations (11)–(16) are normally carried out by numerical quadrature. In Figure 3, it is seen that around each node (an open circle), say the I_p th node, there is a cluster (a shaded area), named ψ_{I_p}. From now on, force calculation is no longer performed at all unit cells in the entire system but in all clusters. A representative unit cell (a black solid square) is the one within one of $\psi_{I_p} = \{l : |\mathbf{X}_l - \mathbf{X}_{I_p}| \leq R_{I_p}\}$. Here, for the sake of presentation we assume there is no overlapping of clusters. If there is an overlap, that means there are some representative unit cells located in the two clusters, we will allocate a representative unit cell to the cluster which is closest to the representative unit cell. $\mathbf{X}_l$ is the position of the lth unit cell, and R_{I_p} is the radius of the cluster ψ_{I_p} centered at the I_pth node. We postulate that the cluster summation rule reads

$$\begin{aligned}
\tilde{\mathrm{F}}_{J}^{\alpha} = & \int_{\Omega(\mathbf{x})} \frac{1}{\Delta V(\mathbf{x})} \Phi_J(\mathbf{x}) \sum_{\beta=1}^{N_a} \int_{\Omega(\mathbf{x}')} \frac{1}{\Delta V(\mathbf{x}')} \mathbf{F}^{\alpha\beta}\Big[\mathbf{\Phi}_I(\mathbf{x})\mathbf{U}_I^{\alpha}, \mathbf{\Phi}_K(\mathbf{x}')\mathbf{U}_K^{\beta}\Big] \mathrm{d}\Omega(\mathbf{x}')\mathbf{d}\Omega(\mathbf{x}) \\
& + \int_{\Omega(\mathbf{x})} \frac{1}{\Delta V(\mathbf{x})} \mathbf{\Phi}_J(\mathbf{x}) \sum_{\beta=1}^{N} \mathbf{F}^{\alpha\beta}[\mathbf{\Phi}_I(\mathbf{x})\mathbf{U}_I^{\alpha}, \mathbf{u}^{\beta}] \mathrm{d}\Omega \\
\approx & \sum_{I_p \in \ell} n_{I_p} \sum_{j \in \psi_{I_p}} \sum_{k=1}^{N_l} \sum_{\beta=1}^{N_a} \mathbf{\Phi}_J(\mathbf{x}_j) \mathbf{F}^{\alpha\beta}\Big[\mathbf{U}_I^{\alpha}\mathbf{\Phi}_I(\mathbf{x}_j), \mathbf{U}_K^{\beta}\mathbf{\Phi}_K(\mathbf{x}_k)\Big] \\
& + \sum_{I_p \in \ell} n_{I_p} \sum_{j \in \psi_{I_p}} \sum_{\beta=1}^{N} \mathbf{\Phi}_J(\mathbf{x}_j) \mathbf{F}^{\alpha\beta}\big[\mathbf{U}_I^{\alpha}\mathbf{\Phi}_I(\mathbf{x}_j), \mathbf{u}^{\beta}\big],
\end{aligned} \tag{17}$$

where n_{I_p} is the weight of the I_pth cluster; ℓ is the set of all nodes, and N_l is the total number of unit cells in the whole system. When the clusters shrink to the size of the rep-cells, i.e. $\psi_{J_p} = \{J_p\}$, it holds $\Phi_I(\mathbf{x}_{J_P}) = \delta_{IJ_p}$, and the cluster summation rule boils down to a node-based summation rule

$$\tilde{\mathbf{F}}_{J}^{\alpha} \approx n_J \sum_{k=1}^{N_l} \sum_{\beta=1}^{N_a} \mathbf{F}^{\alpha\beta}\Big[\mathbf{U}_J^{\alpha}, \mathbf{U}_K^{\beta}\Phi_K(\mathbf{x}_k)\Big] + n_J \sum_{\beta=1}^{N} \mathbf{F}^{\alpha\beta}\big[\mathbf{U}_J^{\alpha}, \mathbf{u}^{\beta}\big]. \tag{18}$$

In this case, the weighting factor is n_J, which is the number of unit cells represented by the Jth node, thus $n_J = \sum_{j=1}^{N_l} \Phi_J(\mathbf{x}_j) \quad \forall J \in \ell$. On the other extreme, $n_J = 1 \ \forall J \in \ell$ implies that all pairs of interatomic forces are calculated. In all cases $\sum_{I_p \in \ell} \sum_{j \in \psi_{I_p}} n_j = N_l$ holds.

Figure 3 shows the details or key points to calculate the interatomic force between any two atoms. The force between any two atoms in the atomic region is treated exactly the same way as in MD simulation. In the continuum region the force between any two atoms in different or same unit cells should be distributed to all the nodes of the elements, in which the two unit cells reside. For example, there is a unit cell l located in cluster ψ_H with weighting factor n_H and another generic unit cell k; $\{\overset{k\alpha}{\mathbf{f}}{}^{l\beta}, \overset{l\beta}{\mathbf{f}}{}^{k\alpha}\}$ represents a pair of interatomic forces acting on the $k\alpha$th atom and the $l\beta$th atom, $\overset{k\alpha}{\mathbf{f}}{}^{l\beta} = -\overset{l\beta}{\mathbf{f}}{}^{k\alpha}$; through shape function $\mathbf{\Phi}_{kI} = \mathbf{\Phi}_I(\mathbf{x}_k)$, force $n_H \mathbf{\Phi}_{kI} \overset{k\alpha}{\mathbf{f}}{}^{l\beta}$ is distributed to the αth atom of node I; similarly, $n_H \mathbf{\Phi}_{kJ} \overset{k\alpha}{\mathbf{f}}{}^{l\beta}$, $n_H \mathbf{\Phi}_{kK} \overset{k\alpha}{\mathbf{f}}{}^{l\beta}$, and $n_H \mathbf{\Phi}_{kL} \overset{k\alpha}{\mathbf{f}}{}^{l\beta}$ are distributed to the αth atom of nodes J, K, and L; in the same way, $n_H \mathbf{\Phi}_{lJ} \overset{l\beta}{\mathbf{f}}{}^{k\alpha}$, $n_H \mathbf{\Phi}_{lK} \overset{l\beta}{\mathbf{f}}{}^{k\alpha}$, $n_H \mathbf{\Phi}_{lG} \overset{l\beta}{\mathbf{f}}{}^{k\alpha}$, and $n_H \mathbf{\Phi}_{lH} \overset{l\beta}{\mathbf{f}}{}^{k\alpha}$ are distributed to the βth atom of nodes J, K, G, and H. Let $\{\overset{m\alpha}{\mathbf{f}}{}^{\gamma}, \overset{\gamma}{\mathbf{f}}{}^{m\alpha}\}$ represent a pair of interatomic forces acting on the $m\alpha$th atom in the continuum region and the γth atom in the atomic region.

4. Wave propagation

In this work, we investigate wave propagating across the interface between atomic region and continuum region; atomic units are used throughout this letter:

$$\begin{aligned}
\text{Mass:} \quad & m_e = 9.10938188 \times 10^{-31}\,\text{kg}, \\
\text{Length:} \quad & a_o = 1\text{Bohr} = 0.529177249 \times 10^{-10}\,\text{m}, \\
\text{Electron charge:} \quad & e = 1.602176462 \times 10^{-19}\,\text{C}, \\
\text{Time:} \quad & \tau_o = 2.418884326 \times 10^{-17}\,\text{s}, \\
\text{Energy:} \quad & E_h = 1\ \text{hartree} = 4.3597482 \times 10^{-18}\,\text{J}.
\end{aligned}$$

The MD model and the AFT model ($2a \times 2a \times 150a$, $a = 7.9368\,\text{Bohr} \approx 0.42\,\text{nm}$) for MgO are schematically illustrated in Figure 4a; the MD model consists of 10,872 atoms and the AFT model consists of 2232 atoms and 48 3-D 8-node FEs with the interface at $z = 30a$. It is noticed that the resolution in the z-direction between atomic region and continuum region has a dramatic change since the size of element is $1a \times 1a \times 10a$. Figures 4a and c shows the boundary conditions and the loading history, respectively.

The Coulomb–Buckingham potentials between pairs of two atoms, Mg – Mg, O – O, Mg – O can be expressed as [17]

$$U^{\xi\eta} = \frac{e^{\xi} e^{\eta}}{r^{\xi\eta}} + A^{\xi\eta} e^{-r^{\xi\eta}/B^{\xi\eta}} - \frac{C^{\xi\eta}}{(r^{\xi\eta})^6}, \tag{19}$$

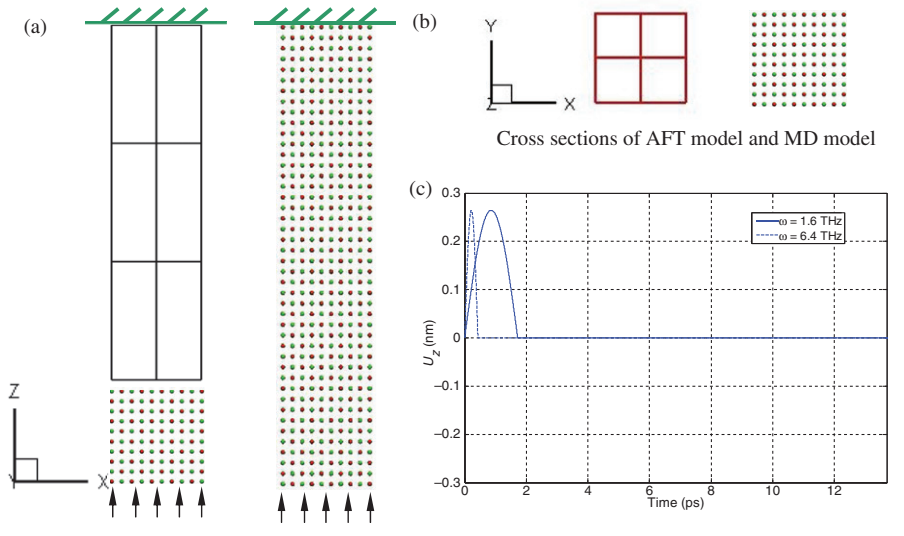

Figure 4. Schematic descriptions of computational model of an MgO specimen under an impulsive loading: (a) AFT model and MD model, (b) cross sections of AFT model and MD model, and (c) loading history.

where $A^{\xi\eta}$, $B^{\xi\eta}$, and $C^{\xi\eta}$ are material constants and $r^{\xi\eta} \equiv \left\|\mathbf{r}^{\xi\eta}\right\| \equiv \left\|\mathbf{r}^{\xi} - \mathbf{r}^{\eta}\right\|$. The material constants used in this work for MgO are

$$M_{\mathrm{Mg}} = 4.57636 \times 10^4 m_e, \quad M_{\mathrm{O}} = 3.01251 \times 10^4 m_e,$$

$$e^{\mathrm{Mg}} = 2e, \quad e^{\mathrm{O}} = -2e,$$

$$A^{\mathrm{Mg-Mg}} = C^{\mathrm{Mg-Mg}} = 0,$$

$$A^{\mathrm{Mg-O}} = 47.2 \text{ hartree}, \quad B^{\mathrm{Mg-O}} = 0.56635 \text{ Bohr}, \quad C^{\mathrm{Mg-O}} = 0,$$
$$A^{\mathrm{O-O}} = 350.88 \text{ hartree},$$
$$B^{\mathrm{O-O}} = 0.41415 \text{ Bohr}, \quad C^{\mathrm{O-O}} = 53.554 \text{ hartree Bohr}^6.$$

Figures 5–7 show the responses of Points $L1\,(a, a, 28a)$, $L2\,(a, a, 70a)$, and $L3\,(a, a, 110a)$, respectively, with three different cluster weighting factors $n_{\min}, n_{\mathrm{mid}}$, and $n_{\max}$ under the compressive impulsive loading with the frequency $\omega \approx 1.6$ THz. Figures 8–10 show the responses of Points $L1\,(a, a, 28a)$, $L2\,(a, a, 70a)$, and $L3\,(a, a, 110a)$, respectively, with three different cluster weighting factors $n_{\min}, n_{\mathrm{mid}}$, and $n_{\max}$ under the compressive impulsive loading with the frequency $\omega \approx 6.4$ THz. Here $n_{\min} = 1$ represents the simulation with all pairs of interatomic forces calculated, i.e., all unit cells in the system are chosen as representative unit cells; $n_{\max}$ represents the simulation with node-based summation rules; n_{mid} $(n_{\min} < n_{\mathrm{mid}} < n_{\max})$ represents the simulation with cluster summation rules.

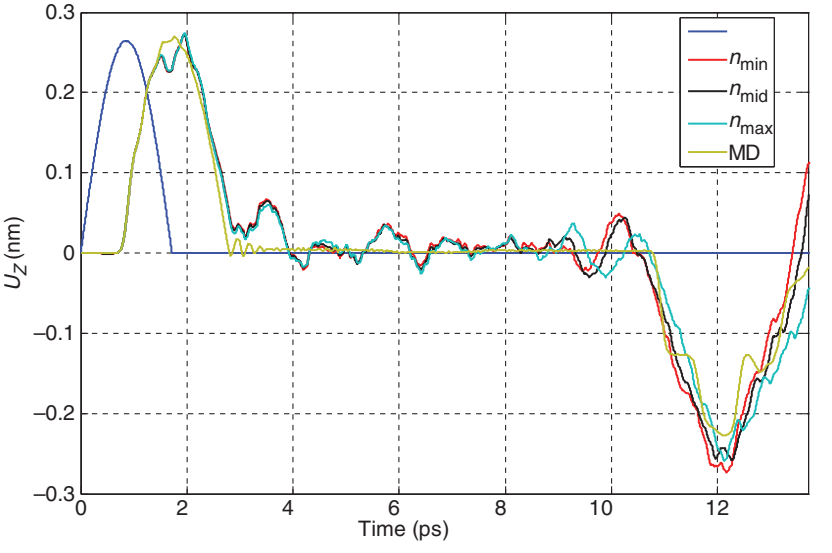

Figure 5. Displacement response of Point $L1$ $(a, a, 28a)$ under the frequency $\omega \approx 1.6$ THz.

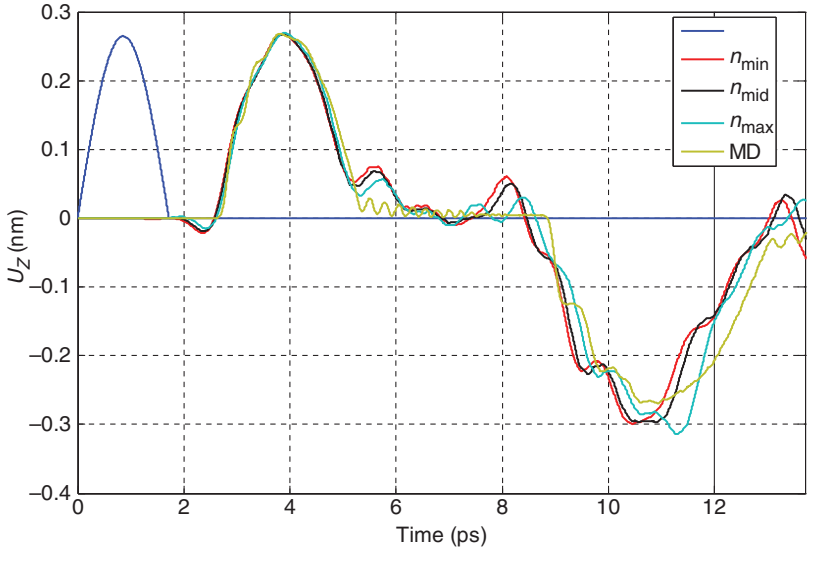

Figure 6. Displacement response of Point $L2$ $(a, a, 70a)$ under the frequency $\omega \approx 1.6$ THz.

The result obtained from MD is considered as a standard and "exact" solution. Since there is no artificial or numerical interface in MD, no reflection happens during the simulation. However, when we adopt the AFT modeling, we have created an artificial interface between atomic region and continuum region just as many other multiscale theories do. If one does not adopt any numerical treatment at the

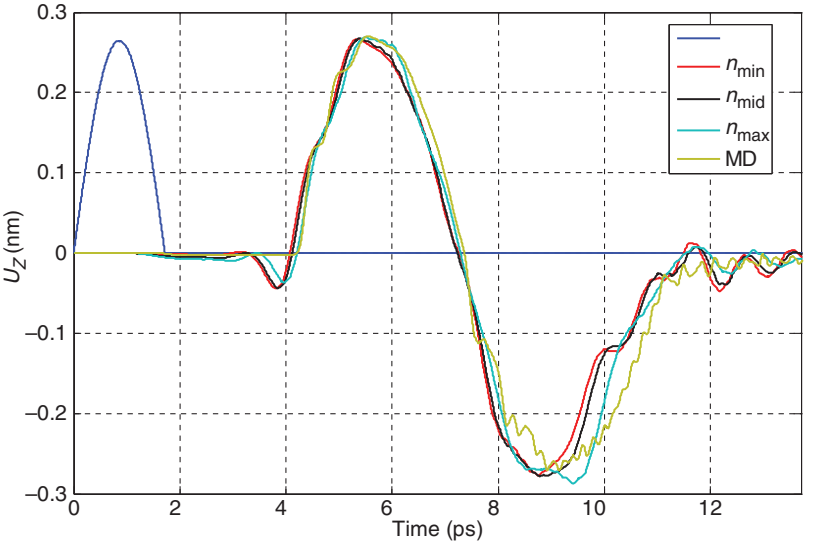

Figure 7. Displacement response of Point $L3$ $(a, a, 110a)$ under the frequency $\omega \approx 1.6\,\text{THz}$.

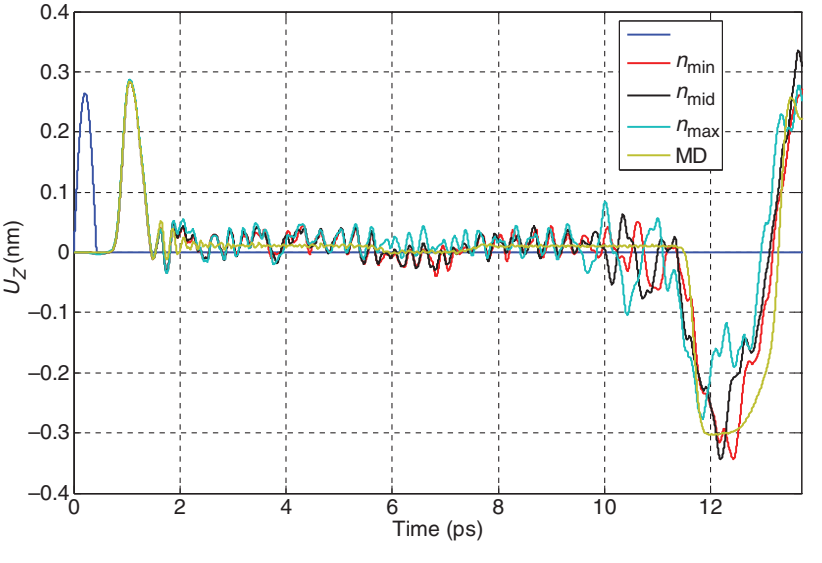

Figure 8. Displacement response of Point $L1$ $(a, a, 28a)$ under the frequency $\omega \approx 6.4\,\text{THz}$.

interface, such as handshaking region, or transition region, the reflection at the interface will happen and dramatically affect the material phenomena during the simulation just like the reflection between fine mesh and coarse mesh in all the FE analyses. In this article, it employs the interatomic forces as the constitutive relation. This nonlocal procedure overcomes the force mismatch between atomic and

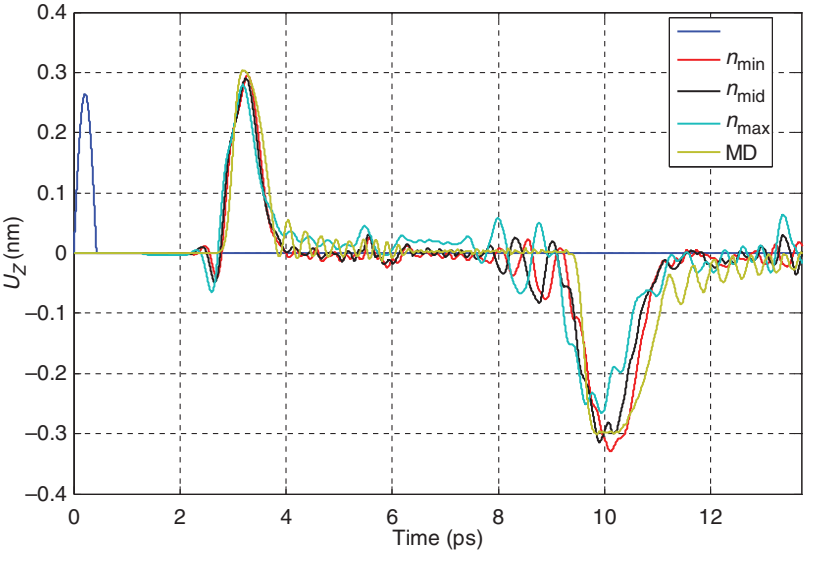

Figure 9. Displacement response of Point $L2$ $(a, a, 70a)$ under the frequency $\omega \approx 6.4\,\text{THz}$.

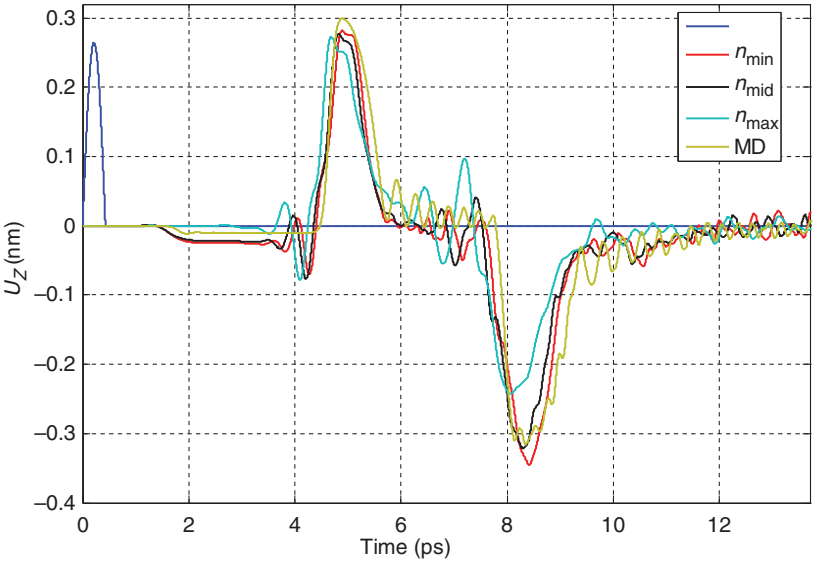

Figure 10. Displacement response of Point $L3$ $(a, a, 110a)$ under the frequency $\omega \approx 6.4\,\text{THz}$.

continuum domains and enables a seamless scale transition between the fully atomistic description and the continuum description. It is clearly seen that the results from AFT are in good agreement with that from MD simulation (cf. Figures 5–7). The downward hooks at $t \approx 4\,\text{ps}$ in Figure 7 from simulations with different

weighting factors n should be considered as deviations from the standard solution from MD simulation. How to improve the numerical solutions further may be a challenge. Also it is noticed that the wave in AFT model passes through the atomic–continuum interface with negligible reflection. As expected, the results with smaller cluster weighting factor are smoother and closer to those from MD simulation. Due to the nonlocality and nonlinearity of the interatomic forces and the finite size of the specimen in the x and y directions, the wave is dispersive. Therefore the frequency of the passing wave becomes smaller than that of the loading impulse.

5. Conclusion

In this letter, we present a new numerical approach for AFT, which offers the possibility to eliminate the spurious wave reflection at the interface between atomic and continuum regions. Furthermore, this approach is completely general and versatile: it can be applied to diversified material problems, including crack propagation, indentations, and grain boundary effects.

References

[1] W. Cai, M. de Koning, V.V. Bulatov and S. Yip, Phys. Rev. Lett. 85 (15) (2000) p.3213.
[2] W. E and Z. Huang, Phys. Rev. Lett. 87 (2001) p.135501.
[3] A.C. To and S. Li, Phys. Rev. B. 72 (3) (2005) p.035414.
[4] S. Li, X. Liu, A. Agrawal and A.C. To, Phys. Rev. B 74 (2006) p.045418.
[5] Y. Chen, J. Chem. Phys 130 (13) (2009) p.134706.
[6] P. Gumbsch, S.J. Zhou and B.L. Holian, Phys. Rev. B 55 (1997) p.3445.
[7] S.J. Carroll, P.D. Nellist, R.E. Palmer, S. Hobday and R. Simth, Phys. Rev. Lett. 84 (2000) p.2654.
[8] M. Moseler, J. Nordiek and H. Haberland, Phys. Rev. B 56 (1997) p.15439.
[9] S.P. Xiao and T. Belytschko, Comput. Methods Appl. Mech. Eng. 193 (2004) p.1645.
[10] G.J. Wagner and W.K. Liu, J. Comput. Phys. 190 (2003) p.249.
[11] Y. Chen and J.D. Lee, Phil. Mag. 85 (2005) p.4095.
[12] J.D. Lee, X. Wang and Y. Chen, Theor. Appl. Fract. Mech. 51 (1) (2009) p.33.
[13] R.J. Hardy, J. Chem. Phys. 76 (1) (1982) p.622.
[14] R. Miller, E.B. Tadmor, R. Phillips and M. Ortiz, Modell. Simul. Mater. Sci. Eng. 6 (1998) p.607.
[15] E.B. Tadmor, R. Phillips and M. Ortiz, Phil. Mag. A 73 (1996) p.1529.
[16] J. Knap and M. Ortiz, J. Mech. Phys. Solids 49 (2001) p.1899.
[17] R.W. Grimes, J. Am. Ceram. Soc. 77 (1994) p.378.